Kinematic Analysis and Dimensional Synthesis of Exechon Parallel Kinematic Machine for Large Volume Machining

Kinematic Analysis and Dimensional Synthesis of Exechon Parallel Kinematic Machine for Large Volume Machining

Y. Jin*
Queen's University Belfast
United Kingdom BT9 5AH
Email: y.jin@qub.ac.uk

Z.M. Bi
Indiana Univ. Purdue Univ.
Fort Wayne, IN46805, USA
Email: biz@ipfw.edu

H.T. Liu
Tianjin University
China 300072
Email: liuhaitao_tju@126.com

C. Higgins
Queen's University Belfast
United Kingdom BT9 5AH
Email: c.j.higgins@qub.ac.uk

M. Price
Queen's University Belfast
United Kingdom BT9 5AH
Email: m.price@qub.ac.uk

W.H. Chen
Beihang University
China 100191
Email: whchen@buaa.edu.cn

T. Huang
Tianjin University
China 300072
Email: tianhuang@tju.edu.cn

ABSTRACT

A parallel kinematic machine (PKM) topology can only give its best performance when its geometrical parameters are optimized. In this paper, dimensional synthesis of a newly developed PKM is presented for the first time. An optimization method is developed with the objective to maximize both workspace volume and global dexterity of the PKM. Results show that the method can effectively identify design parameter changes under different weighted objectives. The PKM with optimized dimensions has a large workspace to footprint ratio and a large well-conditioned workspace, hence justifies its suitability for large volume machining.

1 Introduction

Large volume manufacturing companies, e.g., aerospace manufacturers, are looking for cost effective flexible solutions to meet the ever increasing customer demands towards high speed and high quality [1]. Parallel kinematic machines (PKMs) show the huge potential to meet these requirements [2], and they have attracted much attention from universities to industries over the last three decades. Numerous types of PKMs have been proposed in literature, but few of them have been successfully commercialized and utilized in production [3]. The major reason for that is the small workspace and the limited flexibility. To overcome these drawbacks while maintaining the merits of high stiffness, speed and accuracy, the current trend in large volume manufacturing is to utilize hybrid parallel kinematic machines (HPKM) for 5-axis machining [4–9]. Research has shown that HPKMs can offer competitive advantages over conventional CNC machines [6],though there is still a long way to go before putting them into productive work, such as large volume high precision manufacturing. The Tricept machine is by far the most successful machine for high stiffness manufacturing, with more than 300 currently in production. Motivated by reducing the number of passive joints and effective utilization of actuator stiffness, the inventor of Tricept, Neumann [6] patented a novel HPKM named Exechon. Queen's University Belfast (QUB) is a research partner with Exechon Corporation to investigate the further design and application of the new machine. The prototyping system has been developed and its improved performance has been demonstrated through our primary experiments [10]. As shown in Fig. 1(a), an integrated HPKM Exechon system has been designed and implemented, and it is constructed by a parallel kinematic architecture connected by a two-DOF (degree of freedom) head at the end. Fig. 1(b) shows a zoomed view of the actual physical model with some joints depicted. The herein paper addresses dimension synthesis of the Exechon PKM (without accounting the 2-DOF wrist), which has one translation DOF and two rotational DOF [11]. This approach not only

(a)

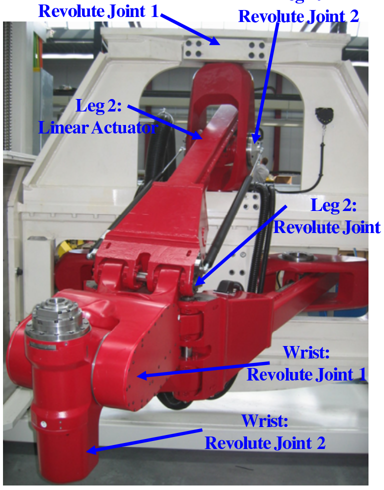

(b)

Fig. 1. Physical model of a 5-DOF hybrid Exechon machine in QUB

help improve existing design and dimensioning of the new series of the machine, but also can be generalized and applied to other PKMs.

PKM design usually involves two steps, i.e., topology synthesis and dimension synthesis (optimization), both of which are important for designing PKMs to achieve specific performance. A good topology can only provide good performance when its geometrical parameters are optimized. The existing methods of dimension synthesis can be classified into two categories, i.e., objective-function based optimal design [12–17]and performance-chart based design [18, 19]. Defining suitable performance indices, reducing the number of design variables, as well as employing proper optimization algorithms, are still challenging issues [20, 21]. Gosselin and Angeles proposed the global conditioning index (GCI) for measuring the global dexterity of manipulators over their entire workspace in design optimization. Liu and Gao [22] studied optimum design of 3-DOF spherical parallel manipulators with respect to the conditioning and stiffness indices. Chablat and Wenger [23] studied architecture optimization of the Orthoglide with prescribed kinetostatic performances in a prescribed workspace. Huang et al. [24] introduced dimension optimization for the TriVariant with two performance indices, i.e., global and comprehensive conditioning indices. Li and Xu [25] introduced a new optimization approach which utilized both the global dexterity index and space utility ratio for design a 3-PUU translational parallel mechanism. Pierrot et al. [26] introduced optimal design of a 4-DOF parallel manipulator with the cost of links as an objective while keeping machine cycle time and dexterity as optimization constraints. Liu et al. [27] designed a HPKM with large workspace/limb-stroke ratio, and a global conditioning index based on the minimum singular value of Jacobian is defined for dimension optimization. Ottaviano and Ceccarelli [28] used specified workspace volume as the design objective for synthesizing the design parameters of the CaPaMan. Jiang and Gosselin [29,30] addressed geometric optimization for achieving maximal singularity-free workspace of several types of parallel mechanisms. Altuzarra et al. [31] studied dimensional synthesis using Pareto-optimization with three design objectives, including workspace volume, dexterity and energy consumption. Wang et al. [32] recently proposed a frame-free index which can effectively evaluate robot transmission capabilities. Although many performance indices have been proposed, construction of the optimization function with suitable indices as well as design variables is not fully addressed [20, 21, 24].

Most literature focuses on design of PKMs with symmetrical architectures associated with pure translation or pure rotational DOF, which makes ease of analysis and dimensional optimization as the Jacobian matrix is homogeneous provided that all actuators are of the same type. This paper deals with the Exechon-PKM which has an asymmetrical architecture and mixed translation/rotational DOF. Therefore a special treatment is proposed in this work to annihilate the non-homogeneity of the Jacobian matrix. An optimization approach is introduced for synthesizing link dimensions of the PKM taking into account of joints motion constraints. Results show that the newly developed method is very useful for identifying the effects of design parameter changes on the PKM performance. The results also show that the Exechon PKM has a large workspace to footprint ratio, and very good conditioning over the whole workspace. This makes it a suitable machine tool for large volume machining, e.g., milling in aircraft assembly.

This paper is organized as follows. Section 2 describes the architecture of the Exechon PKM. Section 3 presents the kinematics of the PKM. Section 4 formulates the generalized Jacobian of the PKM. Sections 5 and 6 give details of the workspace analysis and dimension optimization respectively. Section 7 concludes this paper.

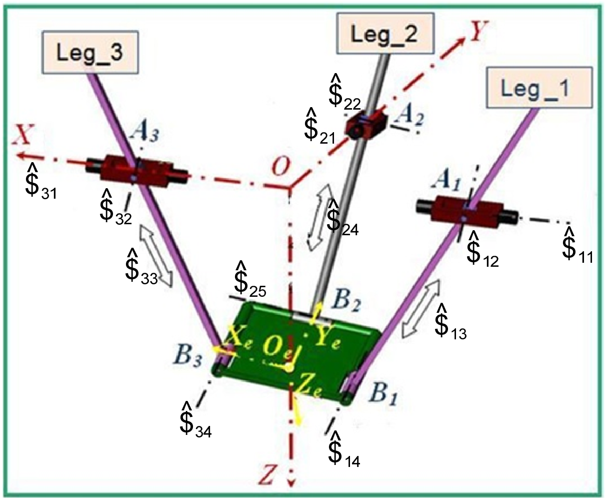

Fig. 2. Schematic diagram of Exechon-PKM

2 Description of the PKM

Figure 2 shows the parallel architecture of the Exechon in which the end-effecter platform is supported by three legs denoted as Leg_1, Leg_2, and Leg_3, respectively. Leg_1 and Leg_3 have an identical architecture in which a universal joint is mounted on the base, linked by a linear actuator and an revolute joint connecting to the moving platform. Leg_2 is slightly different from Leg_1 and Leg_3 as it has one more rotary DOF about the actuator axis. Kinematically, Leg_2 can be regarded as being constructed by an spherical joint on the base, linked by the linear actuator and a revolute joint connecting to the moving platform. At home position, Leg_1 and Leg_3 are symmetrical with respect to Leg_2. Assume points A_i and B_i $(i = 1,2,3)$ denote the attachment points at the corresponding joint centers to the base and the moving platform respectively. The base coordinate system $O - xyz$ is defined as shown in Fig. 2. Point O is the central point of A_1A_3, x-axis points from A_1 to A_3. y-axis is perpendicular to A_1A_3 and towards A_2, z-axis is obtained by right-hand rule. Similarly, the platform coordinate system $O_e - x_ey_ez_e$ is also defined as shown in Fig. 2. Point O_e is the central point of B_1B_3, x_e-axis points from B_1 to B_3. y_e-axis is perpendicular to B_1B_3 and towards B_2, z_e-axis can then be obtained by right-hand rule. Let $\hat{\$}_{ij}$ (s_{ij}) represent a unit screw (vector) along the j^{th} joint of the i^{th} leg, the geometrical constraints of the architecture can be described as follows.

- s_{12}, s_{14}, s_{34} and s_{32} are parallel to each other;
- s_{11} and s_{31} are coincident;
- Actuator axes s_{i3} $(i = 1,3)$ are perpendicular to both s_{i4} and s_{i2};
- Actuator axis s_{24} is perpendicular to both s_{25} and s_{22};

Mobility analysis [11] showed that both Leg_1 and Leg_3 provide one moment wrench $T_i(i = 1,2)$ along Z-axis and one force wrench $f_i(i = 1,2)$ along the second axis of each leg respectively, as shown in Fig. 2. Because of $f_1 \parallel f_2$, $T_1 \parallel T_2$ and $f_i \perp T_i, (i = 1,2)$, the four wrenches form a 2-system composed of the two force wrenches. Therefore, only one constraint, which is independent to the existing two resulted from Leg_1 and Leg_3, is required to obtain three DOFs on the end-effector. In the Exechon PKM, Leg_2 provides a force constraint f_3 which passes through point A_2 and is parallel to $\hat{\$}_{25}$ as shown in Fig. 2. Hence the platform is constrained by three forces which are parallel to the platform plane. As a result, the end-effector will have three DOFs including one translation along z direction and two rotations about x and y axes, respectively.

3 Kinematics

Both the inverse and forward kinematics of this Exechon-PKM have been studied by Bi and Jin [7, 11]. The inverse kinematics of the Exechon hybrid parallel-serial architecture was also recently studied by Zoppi et al. [33]. It is found that only one unique solution exists for the inverse kinematics of the Exechon PKM. This makes ease of control and is regarded as one advantage of this PKM architecture as most PKMs have multiple inverse kinematic solutions.

4 Dimensionally Homogeneous Jacobian

The conventional Jacobian matrix was formulated as a 3×6 matrix by Jin et al. [11]. The analysis shows that no singular configuration exists when the physical constraints of the PKM are taken into account. Zlatanov et al. [34] conducted a thorough analysis of the Exechon-PKM without any physical constraint, and found that several singular configurations may occur. As the Jacobian matrix is used to transform both the velocity and the force systems from the actuator input to moving platform output, its condition is of great interest in design. The condition index C_I of a Jacobian matrix is often used to evaluate the kinetostatic performance of a manipulator. It can represent not only the occurrence of the singular point, but also represents the uniformity of the force distribution with the homogeneous actuator input. The larger the condition index, the better the kinetostatic performance. However, care must be taken when applying the condition index in design, because the elements of Jacobin matrix will have inhomogeneous units when the moving platform motion includes both rotation and translation (no physical unit for orientation but physical unit for position such as meter). To tackle this problem, Tandirci et al. [35] proposed the concept of characteristic length, in which the entries of the Jacobian matrix are divided to render it dimensionless and of a minimum condition number at a posture found by an optimization procedure. This approach was later generalized by Stocco et al. [36] by using two scaling matrices to normalize the Jacobian matrix and balancing the nonuniform capabilities of actuators for task-based design. Liu et al. [37] also formulated a dimensionally homogenous Jacobian in a square matrix of order f (number of DOFs of the PKM) based on generalized Jacobian [38]. As the Exechon-PKM have two rotational DOFs about x- and y- axes respectively, and one translational DOF along z-axis, the conventional Jacobian cannot be used directly to evaluate its conditioning. Since the PKM is used to provide positioning, the kinematic performance at the reference point O_e is of great interest, since the point is directly related to the machining task and understanding its performance will be useful for trajectory planning and control. A special treatment is conducted for formulating the dimensionally homogenous Jacobian as follows. Note that all twists will be represented in the platform coordinate system $O_e - x_e y_e z_e$, so that v of the instantaneous twist $\$_t = \begin{bmatrix} w \\ v \end{bmatrix}$ of the moving platform represents the instantaneous linear velocity of the point O_e.

$\$_t$ can be expressed for legs 1 and 3 as

$$\$_t = \Sigma_{j=1}^{4} \delta\rho_{a,i,j_a} s_{ta,i,j_c} + \Sigma_{j=1}^{2} \delta\rho_{c,i,j_c} s_{tc,i,j} \quad i\text{=1,3;} \tag{1}$$

and for leg 2 as

$$\$_t = \Sigma_{j_a=1}^{5} \delta\rho_{a,2,j_a} s_{ta,2,j_a} + \delta\rho_{c,2,1} s_{tc,2,1} \tag{2}$$

where s_{ta,i,j_a} and $\delta\rho_{a,i,j_a}$ (s_{tc,i,j_c} and $\delta\rho_{c,i,j_c}$) represent the j_ath (j_cth) unit screw of permissions (restrictions) and its intensity within the ith limb. The four unit joint screws of permissions in legs 1 and 3 can be written as:

$$\hat{\$}_{ta,i,1} = \begin{bmatrix} s_{i1} \\ O_eA_i \times s_{i1} \end{bmatrix}, \ \hat{\$}_{ta,i,2} = \begin{bmatrix} s_{i2} \\ O_eA_i \times s_{i2} \end{bmatrix},$$

$$\hat{\$}_{ta,i,3} = \begin{bmatrix} 0 \\ s_{i3} \end{bmatrix}, \ \hat{\$}_{ta,i,4} = \begin{bmatrix} s_{i2} \\ O_eB_i \times s_{i2} \end{bmatrix}, \quad i\text{=1, 3.}$$

The unit wrench of constraints associated with legs 1 and 3 can be obtained as follows.

$$\hat{\$}_{wc,i,1} = \begin{bmatrix} 0 \\ n_{i1} \end{bmatrix}, \ \hat{\$}_{wc,i,2} = \begin{bmatrix} s_{i2} \\ O_eA_i \times s_{i2} \end{bmatrix}, \quad i\text{=1, 3.}$$

where $n_{i1} = s_{i1} \times s_{i2}$. Let the actuated joint in leg i be locked, $\hat{\$}_{wa,i,3}$, which is orthogonal to $\hat{\$}_{ta,i,j_a}$ ($j_a = 1,2,4$ and dual to $\hat{\$}_{ta,j,3}$, can be identified as

$$\hat{\$}_{wa,i,3} = \begin{bmatrix} s_{i3} \\ O_eB_i \times s_{i3} \end{bmatrix}, i = 1,3.$$

With the constraint provided by $\hat{\$}_{wc,i,1}$ and $\hat{\$}_{wc,i,2}$ being released, the unit screw of restrictions, $\hat{\$}_{tc,i,1}$ and $\hat{\$}_{tc,i,2}$, which are orthogonal to $\hat{\$}_{wa,i,3}$ and duel to $\hat{\$}_{wc,i,1}$ and $\hat{\$}_{wc,i,2}$ respectively, can be identified as follows.

$$\hat{\$}_{tc,i,1} = \begin{bmatrix} n_{i1} \\ O_eA_i \times n_{i1} \end{bmatrix}, \ \hat{\$}_{tc,i,2} = \begin{bmatrix} 0 \\ s_{i2} \end{bmatrix}, \quad i\text{=1, 3.}$$

For leg 2, the unit screws of permissions can be generated as

$$\hat{\$}_{ta,2,1} = \begin{bmatrix} s_{21} \\ O_eA_2 \times s_{21} \end{bmatrix},\ \hat{\$}_{ta,2,2} = \begin{bmatrix} s_{22} \\ O_eA_2 \times s_{22} \end{bmatrix},\ \hat{\$}_{ta,2,3} = \begin{bmatrix} s_{24} \\ O_eA_2 \times s_{24} \end{bmatrix},$$

$$\hat{\$}_{ta,2,4} = \begin{bmatrix} 0 \\ s_{24} \end{bmatrix},\ \hat{\$}_{ta,2,5} = \begin{bmatrix} s_{25} \\ O_eB_2 \times s_{25} \end{bmatrix}.$$

The unit wrench of constraints can be obtained as follows.

$$\hat{\$}_{wc,2,1} = \begin{bmatrix} s_{25} \\ O_eA_2 \times s_{25} \end{bmatrix}. \tag{3}$$

Let the actuated joint in leg 2 be locked: the unit wrench, $\hat{\$}_{wa,2,4}$,which is orthogonal to $\hat{\$}_{ta,2,j_a}$ $(j_a = 1,2,3,5)$ and dual to $\hat{\$}_{ta,2,3}$ can be identified as

$$\hat{\$}_{wa,2,4} = \begin{bmatrix} s_{24} \\ O_eB_2 \times s_{24} \end{bmatrix}. \tag{4}$$

When the constraint provided by $\hat{\$}_{wc,2,1}$ is released, the unit screw of restrictions, $\hat{\$}_{tc,2,1}$ which is orthogonal to $\hat{\$}_{wa,2,4}$ and dual to $\hat{\$}_{wc,2,1}$, can be identified as follows.

$$\hat{\$}_{tc,2,1} = \begin{bmatrix} 0 \\ s_{25} \end{bmatrix} \tag{5}$$

For legs 1 and 3, taking orthogonal product on both sides of (1) and (2) by $\hat{\$}_{wa,i,3}$ and $\hat{\$}_{wc,i,j_c}$ $(j_c = 1,2)$ respectively, the following equations are obtained.

$$\hat{\$}_{wa,i,3} \circ \$_t = \delta\rho_{a,i,3}, \quad i_a\text{=1, 3.} \tag{6}$$

$$\hat{\$}_{wc,i,j_c} \circ \$_t = \delta\rho_{c,i,j_c}, \quad i_a\text{=1, 3; } j_c\text{=1,2.} \tag{7}$$

Similarly for leg 2, we have

$$\hat{\$}_{wa,2,4} \circ \$_t = \delta\rho_{a,2,4}, \tag{8}$$

$$\hat{\$}_{wc,2,1} \circ \$_t = \delta\rho_{c,2,1}. \tag{9}$$

As a result, eight equations are obtained from equations (6-9). As only two wrench constraints are resulted from legs 1 and 3, only two equations are needed from (7). Rewriting equations (6)-(9) in matrix form leads to

$$J\$_t = \delta\rho, \tag{10}$$

where

$$J = \begin{bmatrix} J_a \\ J_c \end{bmatrix},\ J_a = \begin{bmatrix} [O_eB_1 \times s_{13}]^T & s_{13}^T \\ [O_eB_2 \times s_{24}]^T & s_{24}^T \\ [O_eB_3 \times s_{33}]^T & s_{33}^T \end{bmatrix},$$

$$J_c = \begin{bmatrix} [O_eA_1 \times s_{12}]^T & s_{12}^T \\ [O_eA_2 \times s_{25}]^T & s_{25}^T \\ [O_eA_3 \times s_{32}]^T & s_{32}^T \end{bmatrix}, \delta\rho = \begin{bmatrix} \delta\rho_{a,1,3} \\ \delta\rho_{a,2,4} \\ \delta\rho_{a,3,3} \\ \delta\rho_{c,1,2} \\ \delta\rho_{c,2,1} \\ \delta\rho_{c,3,2} \end{bmatrix}.$$

In velocity analysis where only the ideal motions of the platform are considered, it reduces to $\$_t = \begin{bmatrix} w \\ v \end{bmatrix}$, $\delta\rho_{a,i,j_a} = \dot{q}_{a,i,j_a}$, which represents the joint rate of the actuator, and $\delta\rho_{c,j_c,i} = 0$. Therefore, by writing J in a partitioned form, equation (10) can be reformulated as

$$\begin{bmatrix} J_{ww} & J_{wv} \\ J_{vw} & J_{vv} \end{bmatrix} \begin{bmatrix} w \\ v \end{bmatrix} = \begin{bmatrix} \dot{q}_a \\ 0 \end{bmatrix}, \tag{11}$$

where $\dot{q}_a = [\dot{q}_{a,1,3} \quad \dot{q}_{a,2,4} \quad \dot{q}_{a,3,3}]^T$. Then taking the linear velocity of point O_e as the independent coordinates, one can obtain

$$J_{pa}v = \dot{q}_a, J_{pa} = J_{wv} - J_{ww}J_{vw}^{-1}J_{vv}, \tag{12}$$

where J_{pa} is the dimensionally homogeneous Jacobian of the mechanism. Although the Jacobian matrix J_{pa} is not frame free, the condition number is a feasible and suitable performance indicator of the PKM at any instantaneous reference point. Therefore, it will be used for dimension optimization in Section 6.

5 Workspace Analysis

The mechanism herein holds a three leg architecture, hence the reachable workspace of the moving platform is formed by intersections of the three reachable workspaces of the three legs. As $\hat{\$}_{11}$ and $\hat{\$}_{31}$ are aligned to each other and points A_1, B_1, O_e, B_3 and A_3 share one common plane, the reachable workspace of point Oe resulted from legs 1 and 3 can be obtained as follows.

rotating one round about joint axis $\hat{\$}_{i2}$ $(i = 1,\ 3)$ with the maximum and minimum leg length from point A_i to point O_e to form two annular areas as shown on the left of Fig. 3.
The interaction area in gray on the left of Fig. 3 is then rotated one round about joint axis $\hat{\$}_{11}$ to form a solid convex, which forms the reachable workspace of point O_e.

Obviously, the maximum and minimum length from point A_i to point O_e can be obtained with the leg fully stretched or retracted as follows.

$$|A_iO_e|_{max} = |A_iB_i|_{max} + |B_iO_e|,$$
$$|A_iO_e|_{min} = |A_iB_i|_{min} - |B_iO_e|.$$

Note that if the result of $|A_iB_i|_{min} - |B_iO_e|$ is negative, $|A_iO_e|_{min}$ should be regarded as zero. As $|A_iO_e|_{min}$ $(i = 1,3)$ is far smaller than $|A_iO_e|_{max}$, the overlapping area is formed by the two big circles in Fig. 3. The two circles can be represented mathematically by:

$$(x - x_{A_i})^2 + (z - z_{A_i})^2 = |A_iO_e|^2_{max} \quad (i = 1,3). \tag{13}$$

Point coordinates $E_i(x_{E_i}, y_{E_i}, z_{E_i})$ $(i = 1,2)$ can then be calculated based on (13). For any point (x_1, z_1) on curve $E_1F_1E_2$, we have

$$z_1 = \pm\sqrt{|A_1O_e|^2_{max} - (x - x_{A_1})^2} + z_{A_1}, \quad for\ x_{E_1} \le x \le x_{F_1}. \tag{14}$$

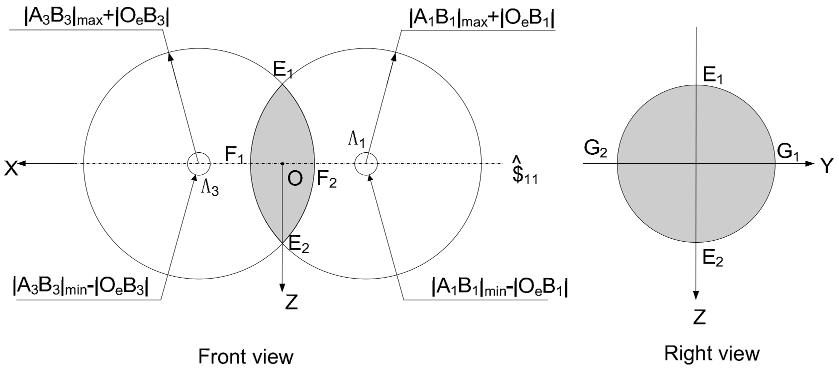

Fig. 3. Reachable workspace of legs 1 and 3 in $x-o-z$ plane

Due to the limits of the second passive rotary joints of both limbs, the negative value of z_1 can be removed. So

$$z_1 = \sqrt{|A_1O_e|^2_{max} - (x-x_{A_1})^2} + z_{A_1}, \quad for\ x_{E_1} \le x \le x_{F_1}. \tag{15}$$

Therefore, the workspace boundary of $E_1F_1E_2$ after rotation about axis $\hat{\$}_{i1}$ can be described as

$$y^2 + z^2 = z_1^2, \quad for\ x_{E_1} \le x \le x_{F_1}. \tag{16}$$

Similarly, the workspace boundary of $E_1F_2E_2$ after rotation about axis $\hat{\$}_{i1}$ can be described as

$$y^2 + z^2 = z_3^2, \quad for\ x_{F_2} \le x \le x_{E_2}, \tag{17}$$

where $z_3 = \sqrt{|A_3O_e|^2_{max} - (x-x_{A_3})^2} + z_{A_3}$.

The maximum axial length $|F_1F_2|$ of the reachable workspace associated with legs 1 and 2 can be represented by

$$\begin{aligned} |F_1F_2| &= 2*(|A_1O_e|_{max} - |A_1A_3|/2) \\ &= 2*(|A_1B_1|_{max} + |B_1O_e| - |A_1A_3|/2). \end{aligned} \tag{18}$$

The maximum radial length $|E_1E_2|$ of the reachable workspace associated with legs 1 and 2 can be represented by

$$|E_1E_2| = \sqrt{|A_1O_e|^2_{max} - (|A_1A_3|/2)^2}. \tag{19}$$

The reachable workspace of point O_e resulted from leg 2 can be represented by a solid spherical shell, which can be described mathematically as

$$|A_2O_e|^2_{min} \le \ (x-x_{A_2})^2 + (y-y_{A_2})^2 + (z-z_{A_2})^2 \ \le |A_2O_e|^2_{max}, \tag{20}$$

where $|A_2O_e|_{max} = |A_2B_2|_{max} + |O_eB_2|$ and $|A_2O_e|_{min} = |A_2B_2|_{min} - |O_eB_2|$. Therefore, the boundary of the shadowed area, i.e. the reachable workspace envelope can be obtained by solving the equation arrays (20) and (16), and (20) and (17), respectively. Figure 4 shows the reachable workspace of the PKM in $x-o-y$ and $y-o-z$ planes, respectively.

To calculate the workspace volume, the reachable workspace can be sliced from top down along z direction, so that the workspace volume of each workspace slice can be integrated along the boundary. The workspace volume can be computed by

$$V = \int_z \int_x [y(G_1\widetilde{F_1}D_1) + y(G_1\widetilde{F_2}D_2) - y(D_1\widetilde{G_3}D_2)] d_x d_z. \tag{21}$$

where $y(G_1\widetilde{F_1}D_1), y(G_1\widetilde{F_2}D_2)$ and $y(D_1\widetilde{G_3}D_2)$ are functions of the three boundary curves in the horizontal plane.

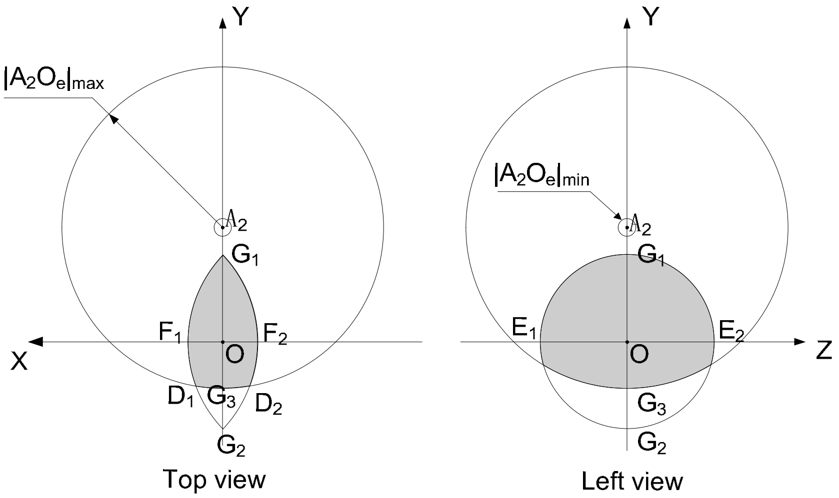

Fig. 4. Reachable workspace of the three legs

6 Dimensional Synthesis

This section will introduce the dimensional synthesis to ensure a good kinematic performance of the PKM.

6.1 Design Parameters

To determine the geometry of the PKM, the following parameters need to be considered.

l_1: the distance between points A_1 and A_3 on the base;
l_2: the distance between the center point of A_1A_3 and point A_2;
l_3: the distance between points B_1 and B_3 on the moving platform;
l_4: the distance between the center point of B_1B_3 and point B_2;
l_s: the stroke of each actuator (assuming all three actuators have the same stroke);
$[l_{min}, l_{max}]$: the motion range of actuators, i.e., the magnitude of A_iB_i, $(i = 1,2,3)$, where $l_{max} = l_{min} + l_s$.

According to the workspace analysis in Section 5, the larger the maximum leg length, the larger the workspace volume. To achieve a good leg stiffness, the l_{min} to l_s ratio should not be larger than 1.5 [9]. Thus it is reasonable to assume herein $l_{min}/l_s = 1.0$. It is also assumed that the ratio of O_eB_2 and B_1B_3 is $l_4/l_3 = 0.75$ for allowing the three attachment points B_i $(i = 1,2,3)$ form a relatively symmetrical triangle. The three normalized variables to be optimized are defined as:

$$\lambda_1 = 0.5 * l_1/l_s, \tag{22}$$

$$\lambda_2 = l_2/l_1, \tag{23}$$

$$\lambda_3 = 2 * l_3/l_1. \tag{24}$$

The numerical coefficients in the above equations are applied for making the three variables λ_1, λ_2 and λ_3 the same magnitude for ease of optimization. To maintain a highly stiff and compact structure, the size of the moving platform is defined smaller than that of the base, and the leg motion range should have a similar magnitude as the longest lateral of the base triangle $A_1A_2A_3$. Based on these considerations, the range of the three variables are defined as follows: $0.5 \le \lambda_1 \le 0.8$, $0.5 \le \lambda_2 \le 1$, $0.5 \le \lambda_3 \le 1$. For passive revolute joint axes s_{i2}, $(i = 1,2,3)$, their physical constraints are within $[-70^\circ, +70^\circ]$. Mathematically, they can be expressed as:

$$-70^\circ \le acos(s_{i1} \cdot u_i) \le +70^\circ. \tag{25}$$

6.2 Objective Function

One disadvantage of PKMs compared with serial robots is their limited workspace. Therefore workspace volume is often taken as the performance measure for dimension optimization of PKMs [28, 31]. Another key performance metric is the global condition index, which is a good indicator of the dexterity of the end-effector in its entire workspace [12–14, 19]. For large volume machining, it is crucial to have a large workspace as well as good conditioning in the entire workspace.

Table 1. Optimization results of the PKM

w_1	λ_1	λ_2	λ_3	V	GCI
1.0	0.5000	0.6397	0.9997	1.3071	0.1500
0.75	0.5000	0.7595	0.9965	1.2619	0.1767
0.5	0.5417	0.9004	0.9704	1.0596	0.2248
0.25	0.7999	0.9742	0.9325	0.5088	0.3560
0	0.8000	0.9902	0.9277	0.4969	0.3572

Therefore the design objective herein is to maximize both the workspace volume V and the global conditioning index GCI, which is defined as follows.

$$Max : F(\lambda_1, \lambda_2, \lambda_3) = w_1 \cdot V + (1 - w_1) \cdot GCI, \tag{26}$$

subject to

$$0.5 \leq \lambda_1 \leq 0.8, \tag{27}$$
$$0.5 \leq \lambda_2 \leq 1.0, \tag{28}$$
$$0.5 \leq \lambda_3 \leq 1.0. \tag{29}$$

where w_1 is weight coefficient. The global condition index [12] is defined as

$$GCI = \frac{\int_V C_I d_V}{\int_V d_V}, \tag{30}$$

where $C_I = 1/(\|J_{pa}\|\|J_{pa}^{-1}\|)$ denotes the local condition index, where $\|\cdot\|$ is referred to as the Euclidean norm of its matrix argument.

6.3 Optimization algorithm and results

The complex optimization [39] is employed to search for the solution in MATLAB environment. The optimization procedure is shown in Fig. 5. For each set of $(\lambda_1, \lambda_2, \lambda_3)$, the objective function is evaluated. The 3-D reachable workspace is divided into a number of layers along z-axis with a resolution of $\Delta z = 0.05$. A number of grids are then generated in each layer with a resolution of $\Delta x = \Delta y = 0.05$. The center point of each grid is then taken as the feature point of the workspace. During the optimization process, all feature points within the workspace resulted from the analytical method in Section 5 will be generated as global known data. In computing the objective function, each of these points is assessed by the inverse kinematic model of the PKM to check if the resulted joint (both active and passive) displacements are within their mechanical limits. If any constraint is violated or the Jacobian matrix is numerically singular ($C_I < 0.1$), the point will be excluded from the workspace. In this way, the effective workspace as well as the GCI can be calculated. After a number of repetitions, the optimal set of $(\lambda_1, \lambda_2, \lambda_3)$ can be obtained. The convergence tolerance is set at $1e-4$ for all design variables and the object function.

Table 1 and Fig. 6 show the optimization results associated with various sets of weights in the objective function. In this case, l_s is set at 0.7. Note that normalized workspace volume $V^* = V/3$ is used for Fig. 6(a), so that it has a similar scale as the GCI values. It is clearly shown in Fig. 6(a) that V decreases when GCI increases. In other words, the two metrics cannot achieve their maximum simultaneously. When the optimization is for maximum V only, i.e. $w_1 = 1$, the largest workspace volume 1.3017 and the lowest GCI value 0.1500 are achieved. When the optimization is for maximizing GCI only, i.e., $w_1 = 0$, the largest GCI value 0.3572 as well as the lowest workspace volume 0.4969 are returned. When the weight coefficient takes intermediate values, both V and GCI are resulted into intermediate values. Figures 6(b) and 6(c) show the trend of λ_i against V and GCI respectively. It clearly shows that with decrease of V or increase of GCI, λ_1 and λ_2 increases while λ_3 decreases. It is also observed maximum V can be achieved by taking minimum λ_1 and λ_2 and maximum λ_3. This leads to a large moving platform associated with a poor dexterity $GCI = 0.1500$. The deviation in GCI values for different weights is within 0.1500 and 0.3572. Depending on the specific application and design constraints, a certain set of optimal design parameters can be selected. The corresponding workspace shape and global conditioning

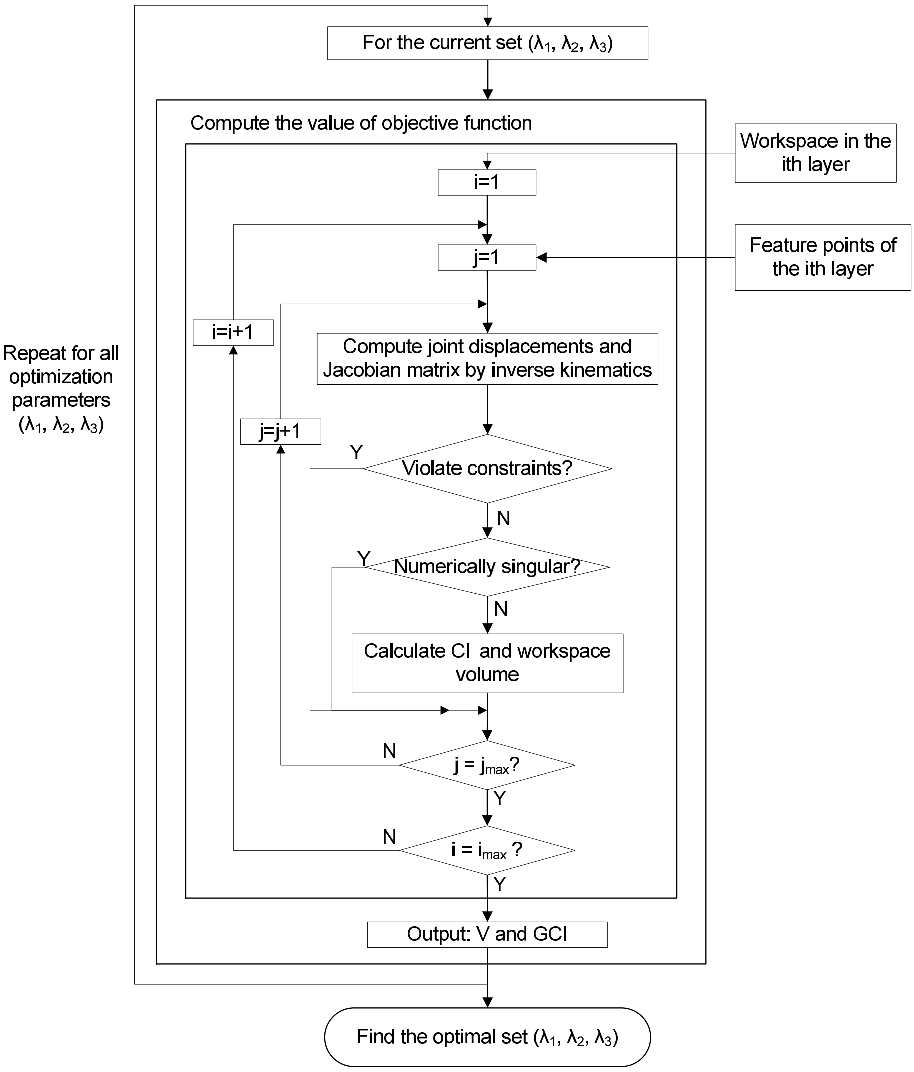

Fig. 5. Optimization procedure of Exechon-PKM

distribution can then be easily obtained. It is worth noting in Fig. 6(a) that the *GCI* curve has its maximum gradient when w_1 is between $[0.5, 0.25]$, where the V curve has also a maximum absolute gradient. Therefore, to achieve a good compromise between V and *GCI*, these values obtained around $w_1 = 0.5$ are recommended. Taking the set of parameters at $w_1 = 0.5$ as an example, its workspace and conditioning atlas relative to the base coordinate frame are shown in Fig. 7 and Fig. 8 respectively. It can be observed that the workspace is in a wedge-like shape with a peach-like section area. The ratio of workspace volume to footprint area is about 4.8 ($= 1.0596/(0.5*0.7*0.7*0.9004), l_s = 0.7$ in this case), which denotes a rather good space utilization. The distribution of condition index is symmetrical about Y-axis, and a large part of the central area in the workspace ($X \in [-0.4, 0.4], Y \in [-0.4, 0.6]$) has a rather good uniform conditioning, i.e. $C_I > 0.25$.

7 Conclusions

This paper is the first study of the dimensional optimization of a PKM that has a non-symmetrical architecture with mixed rotational and translational DOF. An optimization approach is developed for dimension synthesis of the Exechon-PKM with the objective to maximize its workspace volume and global conditioning taking into consideration of the physical joints' limits. The dimensionally homogeneous Jacobian is formulated. Workspace envelope of the PKM is obtained by a geometrical approach, and the reachable workspace volume is modeled by an analytical method. Optimization results show that the optimization algorithm is valid in design with various sets of weights in the performance function. Results also show that the PKM has a large workspace to footprint ratio. The workspace has a rather good uniform conditioning which is suitable for large volume machining tasks. The presented research shows this PKM has great potential for the industrial demands today and future.

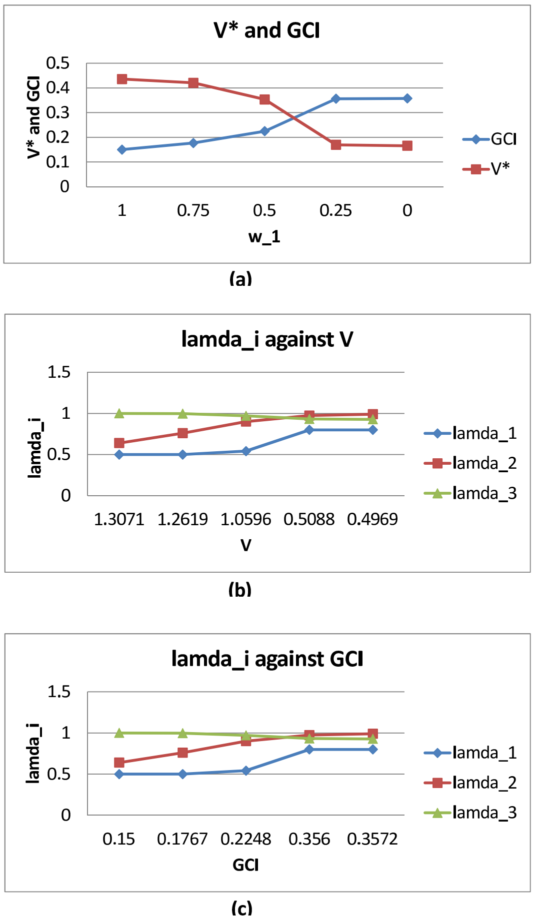

Fig. 6. Optimization results of Exechon PKM

Acknowledgements

The authors gratefully acknowledge the help from the team members and industrial partners of the PKAAA project. Funding support from EPSRC (EP/K004964/1), Investment Northern Ireland (ref.ST_270), NSF China (51420105007) are acknowledged. This research is also partially supported by the Alexander von Humboldt (AvH) Foundation of Germany.

References

[1] Summers, M., 2005. "Robot capability test and development of industrial robot positioning system for the aerospace industry". In SAE Aerospace Manufacturing and Automated Fastening Conference, pp. 2005–01–3336.

[2] Weck, M., and Staimer, D., 2002. "Parallel kinematic machine tools current state and future potentials". *CIRP Annals - Manufacturing Technology,* **51**(2), pp. 671–683.

[3] Rehsteiner, F., Neugebauer, R., Spiewak, S., and Wieland, F., 1999. "Putting parallel kinematics machines (pkm) to productive work". *CIRP Annals - Manufacturing Technology,* **48**(1), pp. 345–350.

[4] Neumann, K., 1988. "Robot, US patent, US4732525".

[5] Tonshoff, H., 1998. "A systematic comparison of parallel kinematics". In First European-American Forum on Parallel Kinematic Machines.

[6] Neumann, K., 2006. "The key to aerospace automation". In SAE Aerospace Manufacturing and Automated Fastening Conference and Exhibition, pp. 2006–01–3144.

[7] Bi, Z., and Jin, Y., 2011. "Kinematic modeling of exechon parallel kinematic machine". *Robotics and Computer Integrated Manufacturing,* **27**, pp. 186–193.

[8] Eastwood, S., 2004. "Error mapping and analysis for hybrid parallel kinematic machines". PhD thesis, Unversity of Nottingham, UK.

[9] Liu, H., Huang, T., Zhao, X., Mei, J., and Chetwynd, D., 2007. "Optimal design of the trivariant robot to achieve a nearly axial symmetry of kinematic performance". *Mechanism and Machine Theory,* **42**(12), pp. 1643–1652.

[10] McToal, P., Jin, Y., Higgins, C., and Brooks, H., 2010. "Alcas wing box root end machining solution - a parallel

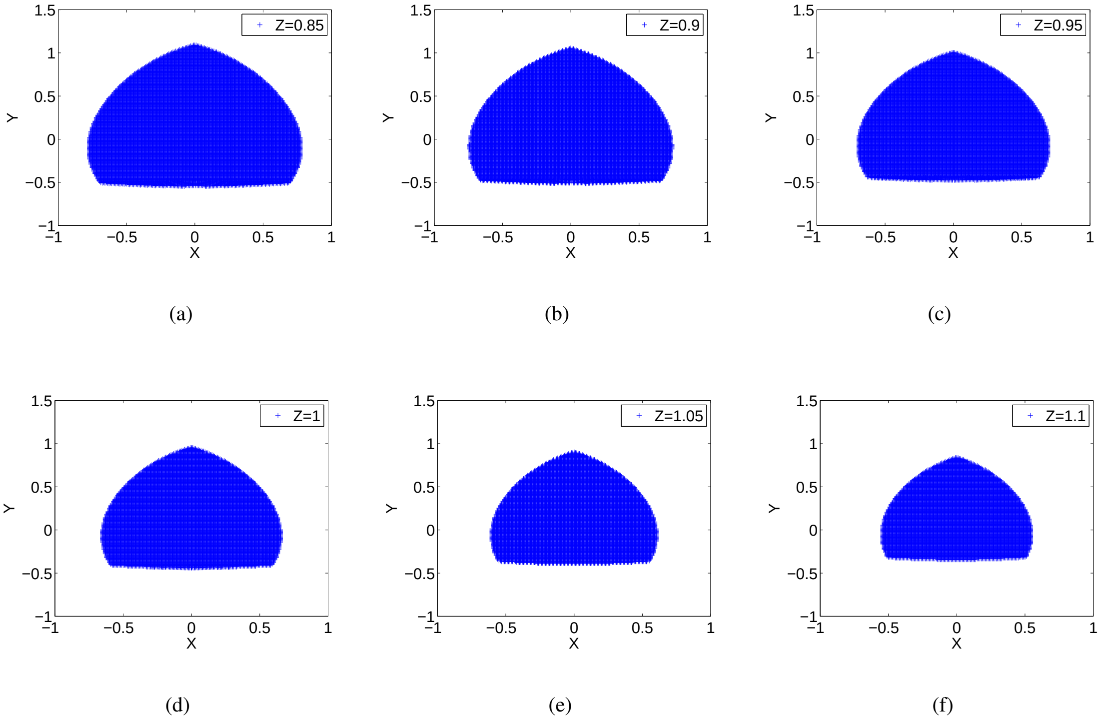

(a) (b) (c)

(d) (e) (f)

Fig. 7. Workspace of the Exechon PKM

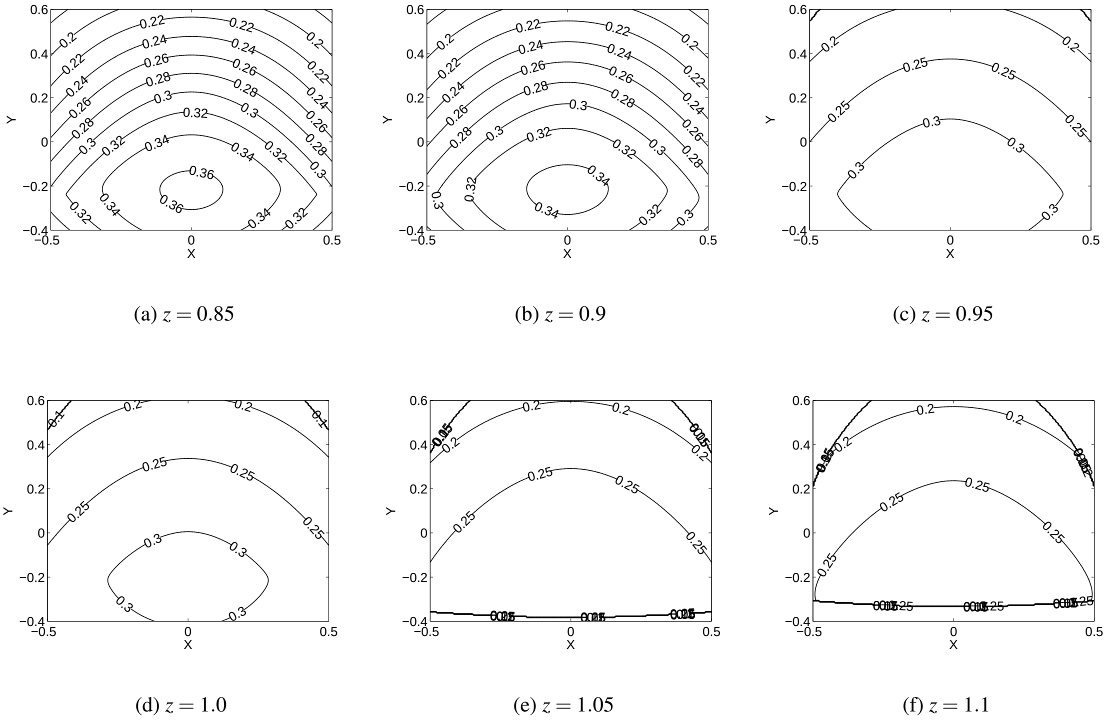

(a) $z = 0.85$ (b) $z = 0.9$ (c) $z = 0.95$

(d) $z = 1.0$ (e) $z = 1.05$ (f) $z = 1.1$

Fig. 8. Conditioning distribution of workspace

kinematic approach". In SAE 2010 Aerospace Manufacturing and Automated Fastening Conference & Exhibition, pp. 10AMAF–0125.

[11] Jin, Y., Bi, Z., Gibson, R., McToal, P., Morgan, M., McClory, C., and Higgins, C., 2011. "Kinematic analysis of a new

over-constrained parallel kinematic machine". In Proceedings of the 13th World Congress in Mechanism and Machine Science, pp. A7–282.

[12] Gosselin, C., and Angeles, J., 1991. "A global performance index for the kinematic optimization of robotic manipulators". *ASME Journal of Mechanical Design,* **113**, pp. 220–226.

[13] Monsarrat, B., and Gosselin, C., 2003. "Workspace analysis and optimal design of a 3-leg 6-dof parallel platform mechanism". *IEEE Transactions on Robotics and Automation,* **19**(6), pp. 954–966.

[14] Castelli, G., Ottaviano, E., and Ceccarelli, M., 2008. "A fairly general algorithm to evaluate workspace characteristics of serial and parallel mnipulators". *Mechanics Based Design of Structures and Machines,* **36**, pp. 14–33.

[15] Jin, Y., Chen, I., and Yang, G., 2006. "Kinematic design of a 6-dof parallel manipulator with decoupled translation and rotation". *IEEE Transactions on Robotics,* **22**(3), pp. 545–551.

[16] Carbone, G., Ottaviano, E., and Ceccarelli, M., 2007. "An optimum design procedure for both serial and parallel manipulators". *Proc. IMechE Part C: J. Mechanical Engineering Science,* **221**, pp. 829–843.

[17] Lou, Y., Liu, G., and Li, Z., 2008. "Randomized optimal design of parallel manipulators". *IEEE Transactions on Automation Science and Engineering,* **5**(2), pp. 223 – 233.

[18] Liu, X., 2006. "Optimal kinematic design of a three translational dofs parallel manipulator". *Robotica,* **24**(2), pp. 239–250.

[19] Liu, X., and Wang, J., 2007. "A new methodology for optimal kinematic design of parallel mechanisms". *Mechanism and Machine Theory,* **42**, pp. 1210–1224.

[20] Merlet, J., 2006. "Jacobian, manipulability, condition number, and accuracy of parallel robots". *ASME Journal of Mechanical Design,* **128**(1), pp. 199–206.

[21] Cardou, P., Bouchard, S., and Gosselin, C., 2010. "Kinematic-sensitivity indices for dimensionally nonhomogeneous jacobian matrices". *IEEE Transactions on Robotics,* **26**(1), pp. 166–173.

[22] Liu, X., and Gao, F., 2000. "Optimum design of 3-dof spherical parallel manipulators with respect to the conditioning and stiffness indices". *Mechanism and Machine Theory,* **35**, pp. 1257–1267.

[23] Chablat, D., and Wenger, P., 2003. "Architecture optimization of a 3-dof translational parallel mechanism for machining applications, the orthoglide". *IEEE Transactions on Robotics and Automation,* **19**(3), pp. 403–410.

[24] Huang, T., Li, M., Zhao, X., Mei, J., Whitehouse, D., and Hu, S., 2005. "Conceptual design and dimensional synthesis for a 3-dof module of the trivariant-a novel 5-dof reconfigurable hybrid robot". *IEEE Transactions on Robotics and Automation,* **21**(3), pp. 449–456.

[25] Li, Y., and Xu, Q., 2006. "A new approach to the architecture optimization of a general 3-puu translational parallel manipulator". *Journal of Intelligent and Robotic Systems,* **46**(1), pp. 59–72.

[26] Pierrot, F., Nabat, V., Krut, S., and Poignet, P., 2009. "Optimal design of a 4-dof parallel manipulator: From academia to industry". *IEEE Transactions on Robotics,* **25**(2), pp. 213–224.

[27] Liu, H., Huang, T., Mei, J., Zhao, X., Chetwynd, D., Li, M., and Hu, S., 2007. "Kinematic design of a 5-dof hybrid robot with large workspace/limbstroke ratio". pp. 530–537.

[28] Ottaviano, E., and Ceccarelli, M., 2002. "Optimal design of capaman (cassino parallel manipulator) with a spefied orientation workspace". *Robotica,* **20**, pp. 159–166.

[29] Jiang, Q., and Gosselin, C., 2009. "Geometric optimization of the mssm gough-stewart platform". *ASME Journal of Mechanisms and Robotics,* **1**(3), pp. 1–8.

[30] Jiang, Q., and Gosselin, C., 2010. "Geometric synthesis of planar 3-rpr parallel mechanisms for singularity-free workspace". *Transactions of the CSME,* **33**(4), pp. 667–678.

[31] Altuzarra, O., Pinto, C., Sandru, B., and Hernandez, A., 2011. "Optimal dimensioning for parallel manipulators: Workspace, dexterity, and energy". *ASME Journal of Mechanical Design,* **133**, April, pp. 041007–1–7.

[32] Wang, J., Wu, C., and Liu, X., 2010. "Performance evaluation of parallel manipulators: Motion/force transmissibility and its index". *Mechanism and Machine Theory,* **45**(10), pp. 1462–1476.

[33] Zoppi, M., Zlatanov, D., and Molfino, R., 2010. "Kinematic analysis of the exechon tripod". In ASME 2010 International DEsign Engineering Technical Conference & Computers and Information in Engineering Conference, pp. 1–8.

[34] Zlatanov, D., Zoppi, M., and Molfino, R., 2012. "Constraint and singularity analysis of the exechon tripod". In ASME 2012 International Design Engineering Technical Conference & Computers and Information in Engineering Conference, pp. 1–10.

[35] Tandirci, M., Angeles, J., and Ranjbaran, F., 1992. "The characteristic point and the characteristic length of robotic manipulators". In Proceedings of ASME 22nd Biennial conference on Robotics, Spatial Mechanisms, and Mechanical Systems, pp. 203–208.

[36] Stocco, L., Sacudean, S., and Sassani, F., 1999. "On the use of scaling matrices for task-specific robot design". *IEEE Transactions on Robotics and Automation,* **15**(5), pp. 958–965.

[37] Liu, H., Huang, T., and Chetwynd, D., 2011. "A method to formulate a dimensionally homogeneous jacobian of parallel manipulators". *IEEE Transactions on Robotics,* **27**(1), pp. 150–156.

[38] Huang, T., Liu, H., and Chetwynd, D., 2011. "Generalized jacobian analysis of lower mobility manipulators". *Mecha-*

nism and Machine Theory, **46**(6), pp. 831–844.
[39] Rao, S., 1996. *Engineering optimization: theory and practice Third Edition*. John Wiley & Sons, New York.

List of the figure and table captions:

Fig. 1: Physical model of a 5-DOF hybrid Exechon machine in QUB
Fig. 2: Schematic diagram of Exechon-PKM
Fig. 3: Reachable workspace of legs 1 and 3 in $x-o-z$ plane
Fig. 4: Reachable workspace of the three legs
Fig. 5: Optimization procedure of Exechon-PKM
Fig. 6: Optimization results of Exechon PKM
Fig. 7: Workspace of the Exechon PKM
Fig. 8: Conditioning distribution of workspace
Table. 1: Optimization results of the PKM